

Understanding the interaction of 14-3-3 proteins with *hDMX* and *hDM2*: a structural and biophysical study

Sonja Srdanović^{1,2}, Madita Wolter^{3,4}, Chi H. Trinh^{1,5}, Christian Ottmann^{3,4} , Stuart L. Warriner^{1,2} and Andrew J. Wilson^{1,2} 

1 Astbury Centre for Structural Molecular Biology, University of Leeds, UK

2 School of Chemistry, University of Leeds, UK

3 Laboratory of Chemical Biology, Department of Biomedical Engineering, Technische Universiteit Eindhoven, The Netherlands

4 Institute for Complex Molecular Systems, Technische Universiteit Eindhoven, The Netherlands

5 School of Molecular and Cellular Biology, University of Leeds, UK

Keywords

14-3-3 proteins; *hDM2* and *hDMX*; p53 pathway; structural biology

Correspondence

A. J. Wilson, School of Chemistry,
University of Leeds, Woodhouse Lane,
Leeds LS2 9JT, UK
Tel: +44 (0)113 3431409
E-mail: a.j.wilson@leeds.ac.uk

(Received 21 December 2021, revised 11
February 2022, accepted 11 March 2022)

doi:10.1111/febs.16433

p53 plays a critical role in regulating diverse biological processes: DNA repair, cell cycle arrest, apoptosis and senescence. The p53 pathway has therefore served as the focus of multiple drug-discovery efforts. p53 is negatively regulated by *hDMX* and *hDM2*; prior studies have identified 14-3-3 proteins as *hDMX* and *hDM2* client proteins. 14-3-3 proteins are adaptor proteins that modulate localization, degradation and interactions of their targets in response to phosphorylation. Thus, 14-3-3 proteins may indirectly modulate the interaction between *hDMX* or *hDM2* and p53 and represent potential targets for modulation of the p53 pathway. In this manuscript, we report on the biophysical and structural characterization of peptide/protein interactions that are representative of the interaction between 14-3-3 and *hDMX* or *hDM2*. The data establish that proximal phosphosites spaced ~20–25 residues apart in both *hDMX* and *hDM2* cooperate to facilitate high-affinity 14-3-3 binding and provide structural insight that can be utilized in future stabilizer/inhibitor discovery efforts.

Introduction

The transcription factor p53 is often described as ‘the guardian of the genome’ because of its central role in regulating diverse biological processes: DNA repair, cell cycle arrest, apoptosis and senescence [1]. Thus, the p53 pathway has seen significant attention in developing new anticancer treatments [2]. One such target has been the interaction between p53 and *hDM2* or *hDMX* (Fig. 1A) [3–5]. p53 is negatively regulated by *hDMX* and *hDM2* [6–10]; they bind to the transactivation

domain of p53 sterically blocking its interaction with DNA [9–12], p53 is additionally targeted for nuclear export and proteasomal degradation through *hDM2* which bears an E3 ligase domain [13–15]. Although *hDMX* lacks such a domain, the E3 ligase activity of *hDM2* is enhanced through formation of *hDMX/hDM2* heterodimers [16–18]. This continuous targeting of p53 for degradation keeps p53 levels low under normal conditions. It is only under stressed conditions (e.g. DNA

Abbreviations

Ahx, aminohexanoic acid; AUC, analytical ultracentrifugation; Boc, Tert-butoxycarbonyl; CD, circular dichroism; DCM, dichloromethane; DIPEA, N,N-Diisopropylethylamine; DMF, dimethylformamide; DMSO, dimethyl sulfoxide; DTT, dithiothreitol; FA, fluorescence anisotropy; FAM, (5,6)-carboxyfluorescein; Fmoc, fluorenylmethoxycarbonyl protecting group; HBS, HEPES-buffered saline; HCTU, (2-(6-Chloro-1H-benzotriazole-1-yl)-1,1,3,3-tetramethylammonium hexafluorophosphate); *hDM2*, human double minute 2 protein; *hDMX*, human double minute 4 protein (*hDM4*); HRMS, high resolution mass spectrometry; IPTG, isopropyl β-d-1-thiogalactopyranoside; ITC, isothermal titration calorimetry; LB, lysogeny broth; p53, tumour suppressor protein 53; SPPS, Fmoc-solid-phase synthesis; SPR, surface plasmon resonance; TCEP, Tris(2-carboxyethyl)phosphine; TFA, trifluoroacetic acid.

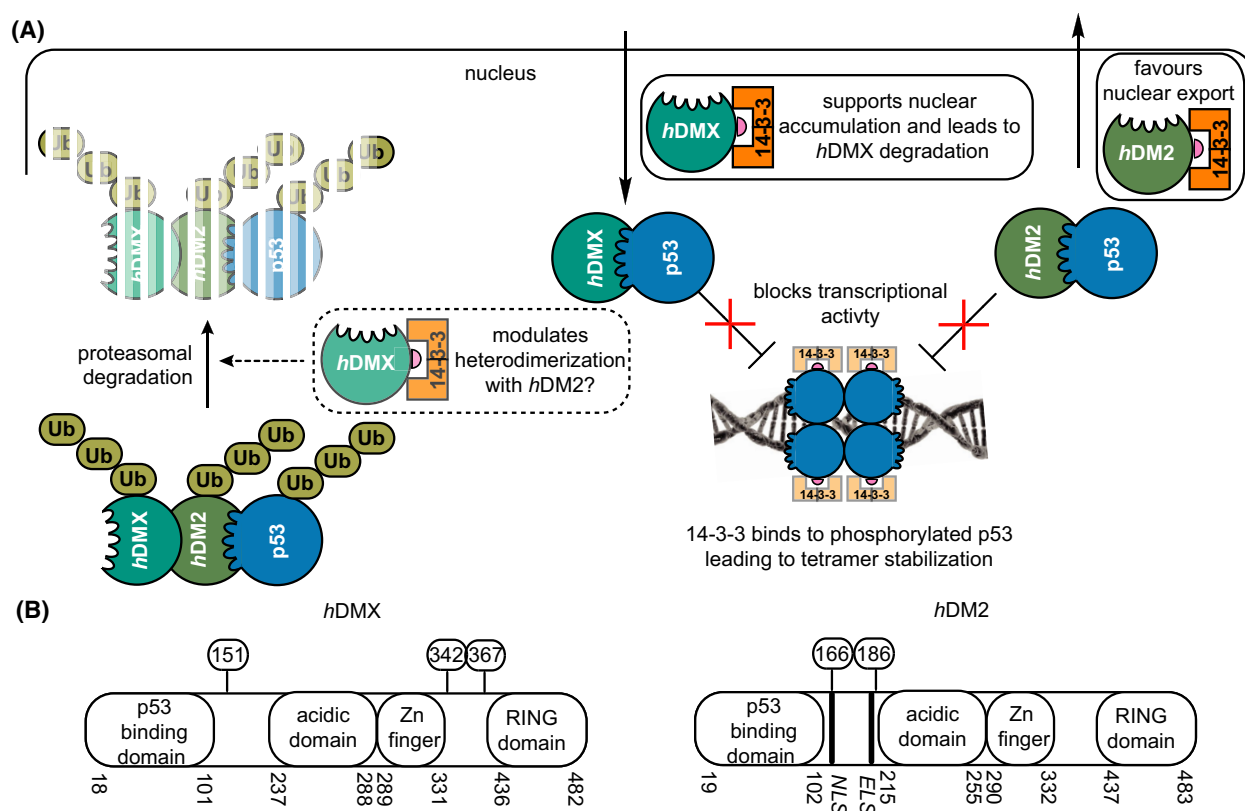


Fig. 1. Negative regulation of the p53 pathway by *hDMX* and *hDM2*: (A) *hDMX* (turquoise) and *hDM2* (green) bind p53 (blue) and subsequently inhibit its transcriptional activity. *hDM2* also facilitates nuclear export of p53, and as a ubiquitin ligase additionally tags p53 for degradation, whilst *hDMX* accelerates *hDM2* mediated ubiquitin ligase activity. 14-3-3 (orange) interacts with: (i) phosphorylated p53 to stabilize tetramer formation, (ii) phosphorylated *hDMX* leading to its nuclear accumulation and degradation, and, possibly modulation of its interaction with *hDM2* and (iii) *hDM2* to facilitate its nuclear export. (B) domain structure of *hDM2* and *hDMX* highlighting phosphosites on *hDM2* and *hDMX* investigated in this work: Ser342 and Ser367 in intracellular localization, protein degradation and ubiquitination, and additionally Ser367 is associated with cell growth and protein stabilization. Ser166 and Ser186 on *hDM2* are involved in apoptosis, signalling pathway regulation and ubiquitination.

damage, hypoxia, oncogene activation and ribosomal stress) that p53 is rapidly activated through multiple post-translational modifications; subsequent stabilization and accumulation of p53 upregulates gene expression leading to cell cycle arrest and/or apoptosis. This tightly controlled autoregulatory loop is thus of vital importance; knockout studies of the oncogenes MDMX and MDM2 (the murine homologues of *hDMX* and *hDM2*) have shown that these proteins are essential in mice studies [19]. However, *hDM2* and *hDMX* are themselves subject to regulatory control and have additional independent roles in cell cycle regulation [20–22]. For instance, in addition to modulating p53 binding, post-translational modification of *hDMX* and *hDM2* such as phosphorylation influences their localization and degradation [21–25].

Several kinases have been reported to phosphorylate *hDMX* and/or *hDM2* whilst cellular studies have

shown that phosphorylated *hDMX* and *hDM2* interact with 14-3-3 [26]. First identified in 1967 [27], 14-3-3 proteins are eukaryotic adapter proteins that control diverse physiological functions through interaction with a large network of proteins, for example, they are involved in signal transduction, protein trafficking, apoptosis and cell cycle regulation [28]. Given these functions, they have been shown to play an important role in inflammatory conditions, neurodegenerative diseases, cancer and cystic fibrosis [29–33]. And have consequently received attention as potential drug-discovery targets [28,34]. The 14-3-3 family of proteins consist of seven isoforms in humans: β , γ , ϵ , η , ζ , σ and τ/θ , all of which share a high degree of sequence conservation [35] (see Fig. S1). Even though sequence conservation between the isoforms can indicate redundancy in protein function, this is not the case for 14-3-3 proteins as different affinities towards a target

protein are clear between the isoforms [36,37]. The 14-3-3 proteins exist as homo or heterodimers where each monomer consists of nine α -helices forming an amphipathic binding groove. Four α -helices are directly responsible for dimer formation, while the rest of the α -helices form the 'W' shape of the protein dimer [38,39]. The N terminal domain of 14-3-3 proteins modulates homo/heterodimerization while the C terminal domain binds client proteins [38]. Activity and modulation of many cellular pathways by 14-3-3 is controlled by phosphorylation events. Target proteins are typically recognized by 14-3-3 through well-defined sequences that can be generalized into three categories: (I) RXX pS/pT XP, (II) RX(Y/F)X pS/pT XP and (III) XX pS/pT X COOH (pS and pT being phosphorylated Ser and Thr, respectively, X being any amino acid). [40] In modes I and II, proline is always located at position +2 in relation to the central pSer/pThr and arginine is at position -3 in mode I. Mode III represents C terminal sequences where pSer/pThr are the penultimate amino acid of the partner protein.

Phosphorylated residues on *hDMX* or *hDM2* are considered relevant to recognition by 14-3-3 proteins, as well as their role in cell signalling is outlined in Fig. 1B [26,41–45]. Relevant sites on *hDMX*: Ser342 and Ser367 are targeted by several kinases (e.g. AMP [45], Akt [41], Chk2 [26,44], or Chk1 [42]). *hDMX* phosphorylation in response to stress or DNA damage with consequent enhancement of *hDM2* mediated *hDMX* degradation has been reported [44,46], together with a role for Ser367 [43]. Phosphorylation of *hDMX* on Ser367 by Chk2 was shown to promote 14-3-3 binding, *hDMX* nuclear import and degradation by *hDM2* [26]. Similarly, Chk1 was shown to phosphorylate *hDMX* at Ser367, to promote 14-3-3/*hDMX* interaction and cytoplasmic retention of *hDMX* to counter *hDMX*-enhanced p53 ubiquitination, leading to its stabilization and activation [42]. However, the potential relevance of both Ser342 and Ser367 to interaction with 14-3-3 has been noted [44,47]. In contrast, Akt has been shown to phosphorylate *hDMX* on Ser367, promoting 14-3-3 binding, stabilizing *hDMX* and consequently enhancing *hDM2* stability leading to suppression of p53 transcriptional activity [41]. Adenosine monophosphate (AMP) mediated phosphorylation of *hDMX* on Ser342 has been shown to induce *hDMX*/14-3-3 interaction resulting in inhibition of p53 ubiquitylation and consequent stabilization [45]. *hDM2* phosphorylation in the NLS/ELS region, by PKB/Akt, can lead to its stabilization [48,49], although the effects are complex; phosphorylation on Ser166 and Ser188 are promoted by Akt kinase [50], and result in positive regulation of *hDM2* by inhibiting its

self-ubiquitination and nuclear translocation [48,51,52]. Phosphorylation at Ser166 and Ser188 does not appear to result in binding of *hDM2* to 14-3-3 [53] whilst such an interaction was observed when phosphorylated at Ser166 and Ser186 by Pim kinase, which simultaneously suppresses phosphorylation of Ser188 [53]. Finally, the interaction between *hDM2* phosphorylated in the ring domain and 14-3-3 σ was observed to accelerate the self ubiquitination of *hDM2*, with a resulting downstream stabilization of p53 [54]. Thus cellular studies have linked *hDMX* and *hDM2* to 14-3-3 proteins; 14-3-3 proteins may indirectly modulate the interaction between *hDMX* or *hDM2* and p53 and represent potential targets for pharmacological modulation of p53 [21,23] but the molecular bases of these interactions remain unexplored. In this manuscript, we report on the biophysical and structural characterization of peptide/protein interactions that are representative of the interaction between 14-3-3 and *hDMX* or *hDM2*. The data reveal the interactions to be mode I [55,56]; whilst such 14-3-3 interactions are not stabilized by typical 14-3-3 interaction stabilizers, for example, Fusicocin and Cotelynin A [57]. These data provide structural insights that could be utilized in future stabilizer/inhibitor discovery efforts. More significantly, our results reveal that in both cases proximal phosphosites spaced ~20–25 residues apart in both *hDMX* and *hDM2* co-operate to facilitate high-affinity 14-3-3 binding and do so through 1:1 stoichiometry.

Results

There are multiple serine and threonine residues in the *hDMX* and *hDM2* proteins that could be phosphorylated (protein sequences with highlighted Ser and Thr residues on *hDMX* and *hDM2*, as well as their alignment [35] can be found in Figs S2 and S3). Therefore, *14-3-3Pred* [58] was used to identify sequences from *hDM2* and *hDMX* that might serve as 14-3-3 binding sequences. *14-3-3Pred* is a webserver that predicts 14-3-3 binding sites in client proteins based on published examples of 14-3-3 interactions with specific amino acids surrounding Ser/Thr. Scores are assigned to each Ser/Thr residue on the protein target whose sequences in FASTA format are queried, using an ensemble approach comprising three different base classification systems: position-specific scoring matrix, support vector machines and artificial neural network. End score values are calculated as the average of three independent methods with a score > 0.5 indicating a high probability of the sequence binding to 14-3-3. The webserver also provides information on the

phosphorylation state for each Ser/Thr residue. The phosphorylated sites on *hDMX* and *hDM2* shown to be relevant for the interaction of 14-3-3 in previous cell-based studies [26,42–45,50,53] were predicted to have a high probability of 14-3-3 binding (Table 1), except pSer342 on *hDMX*, which showed a low probability of binding (score 0.19) whereas Ser151 on *hDMX* – a previously unreported site of phosphorylation – was predicted to be a potential 14-3-3 binding site (score 0.75).

Using the *14-3-3Pred* results server, several key regions of *hDMX* and *hDM2* were thus identified. Peptides containing these binding regions were designed bearing five/six residues flanking the central phosphorylated residue on either side and prepared by solid-phase peptide synthesis (SPPS). Given the proximity of pSer342 and pSer367 from *hDMX*, as well as pSer166 and pSer186 from *hDM2*, we also prepared doubly phosphorylated sequences for both to probe for avidity effects. Peptides were synthesized using a combination of manual or automated Fmoc SPPS on rink amide resin (Rink amide ProTide for doubly phosphorylated sequences) and modified at the N terminus by acetylation for isothermal titration calorimetry (ITC), surface plasmon resonance (SPR) and crystallography studies or with 5,6-carboxyfluorescein following an Ahx linker to function as a tracer in fluorescence anisotropy (FA) assays (Table 1 for peptide sequences, see Table S1 for peptide characterization).

Biophysical characterization of the interaction of *hDMX* and *hDM2* peptides with 14-3-3

To determine the binding affinity between all 7 isoforms of 14-3-3 proteins and *hDMX* and *hDM2* peptides, FA experiments were carried out. 14-3-3 proteins were titrated against a constant concentration of the tracer resulting in an increase of anisotropy upon engaging 14-3-3 proteins (Fig. 2A–C for 14-3-3 binding *hDMX* sequences and Figs S4–S6, for 14-3-3 binding

hDM2 sequences, non-binding sequence, and unphosphorylated controls). A noteworthy feature of the data is that different maximum anisotropy levels were observed between *hDMX* or *hDM2* peptides and 14-3-3 isoforms, indicating different diffusion properties of the fluorophore when bound to the different 14-3-3 isoforms. This may: (a) reflect differences in the interaction between fluorophore and protein [59] restricting the former's mobility to a greater or lesser degree between isoforms or (b) arise as a consequence of a more complex equilibrium, for example, isoform dependent variation in 14-3-3 dimerization [60] across the concentration range of the assay. This will be investigated in future studies. The consequence of this behaviour is that for weaker binding peptides where saturation was not observed, it was not possible to determine a K_d value. Thus, in some cases, for example, $hDM2_{180-192}^{pSer186}$, K_d values (see below) with τ , σ and ϵ could only be estimated to be greater than limiting values. Similarly, accurate fitting for doubly phosphorylated peptides could be obtained only for η , γ and β isoforms. Peptides $hDMX_{335-349}^{pSer342}$ and $hDMX_{361-374}^{pSer367}$ showed affinity for 14-3-3 proteins, whereas peptide $hDMX_{144-158}^{pThr151}$ exhibited no response under the conditions of the assay (see Fig. S5). None of the corresponding unphosphorylated control *hDMX* sequences exhibited evidence of binding under the conditions of the assay confirming the role of phosphorylation for binding of pSer342 and pSer367 to 14-3-3 (see Fig. S6). *hDM2* peptides representing sites pSer166 and pSer186 showed low micromolar affinities to all 14-3-3 isoforms (Fig. S4).

Generally, all peptides exhibited tightest binding towards the 14-3-3 η isoforms, followed by γ , β , τ , ζ , σ , and ϵ , respectively. *hDMX* and *hDM2* peptides mimicking one phosphorylation site fit well to a 1 : 1 binding isotherm. In this previously described model, each 14-3-3 dimer protein can bind two peptides, one peptide per 14-3-3 protomer [38]. K_d values for all 14-3-3 isoforms are reported in Table 2, but for simplicity, only the 14-

Table 1. 14-3-3 binding *hDM2* and *hDMX* Sequences studied.

	Sequence ^a	14-3-3-Pred Score
<i>hDMX</i> ₁₄₄₋₁₅₈ ^{pThr151}	X-STSRKRT pT EDDIPTL-NH2	0.75
<i>hDMX</i> ₃₃₅₋₃₄₉ ^{pSer342}	X-SKLTHSL pS TSDITAI-NH2	0.19
<i>hDMX</i> ₃₆₁₋₃₇₄ ^{pSer367}	X-DCRRTI pS APVVRPK-NH2	1.28
<i>hDMX</i> ₃₃₅₋₃₇₃ ^{pSer342/pSer367}	X-SKLTHSL pS TSDITAIPEKENEKENDVPDCRRTI pS APVVRP-NH2	N/A
<i>hDM2</i> ₁₆₀₋₁₇₁ ^{Ser166}	X-SRRRAI pS ETEEN-NH2	1.10
<i>hDM2</i> ₁₈₀₋₁₉₂ ^{pSer186}	X-QRKRHK pS DSISLS-NH2	0.88
<i>hDM2</i> ₁₆₀₋₁₉₂ ^{pSer166/pSer186}	X-SRRRAI pS ETEENSDELSEGERQRKRHK pS DSISLS-NH2	N/A

^aX = acetyl or FAM-Ahx where FAM is 5,6-carboxyfluorescein and Ahx is aminohexanoic acid.

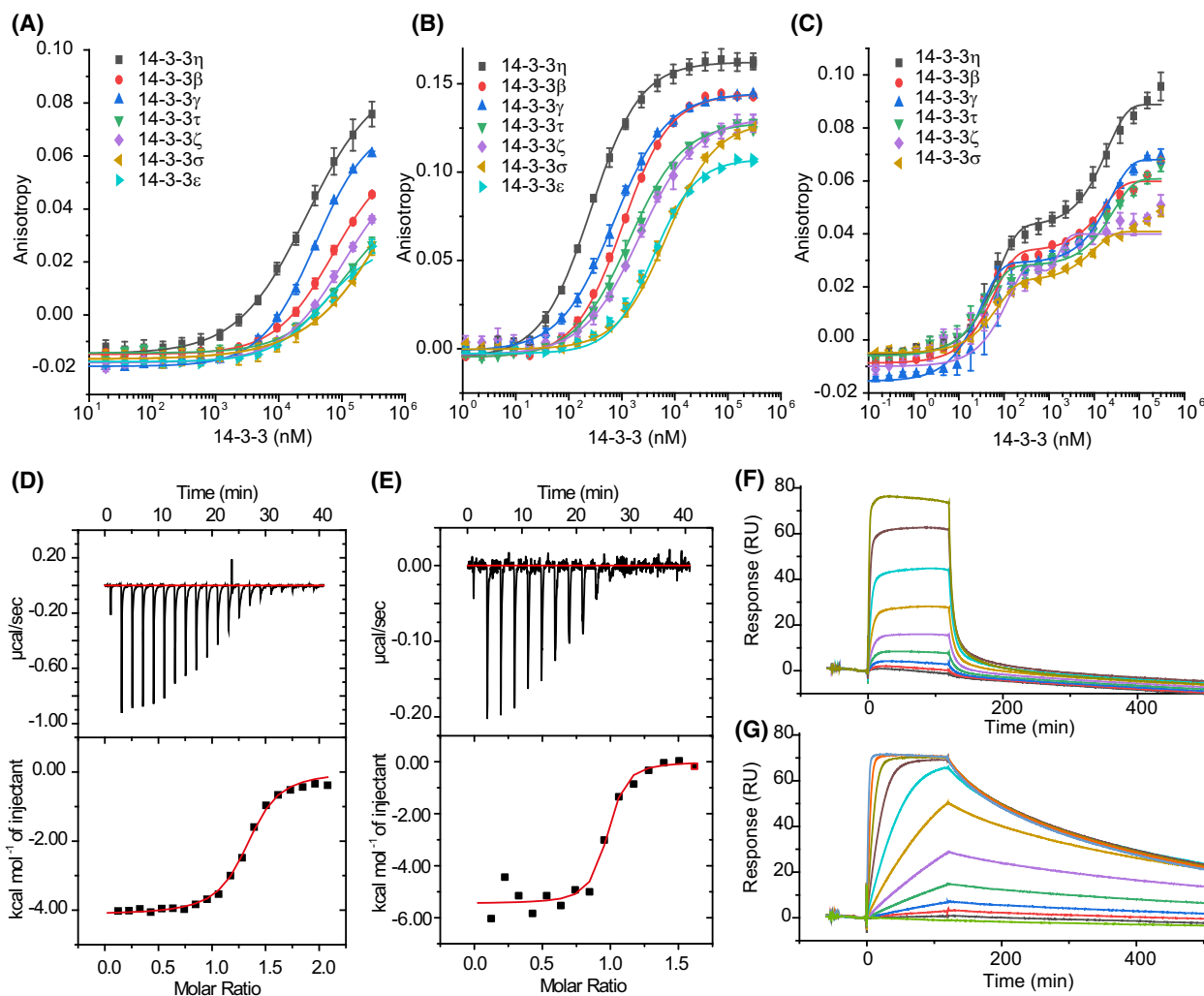


Fig. 2. Biophysical analyses of the interaction between 14-3-3 and hDMX peptides (A–C) FA assays for the hDMX peptides (A) hDMX₃₃₅₋₃₄₉^{pSer342} (B) hDMX₃₆₁₋₃₇₄^{pSer367} and (C) hDMX₃₃₅₋₃₇₃^{pSer342/pSer367} with all isoforms of 14-3-3 (FAM tracer peptide 50 nM, in 10 mM HEPES, 150 mM NaCl, 0.1% Tween 20, 0.1% BSA, pH 7.4, concentration of proteins given as 14-3-3 monomer concentration, error bars represent SD for $n = 3$ replicates); (D, E) ITC data for the interaction of hDMX peptides with 14-3-3η; (D) hDMX₃₆₁₋₃₇₄^{pSer367}; (E) hDMX₃₃₅₋₃₇₃^{pSer342/pSer367} (peptides were titrated into 14-3-3η (0.1 M for mono phosphorylated peptide and 0.02 M for doubly phosphorylated peptide), 25 °C, 25 mM HEPES pH 7.5, 100 mM NaCl, 10 mM MgCl₂, 0.5 mM TCEP); (F, G) Dose–response SPR experiments for the binding of hDMX peptides to immobilized 14-3-3η (F) hDMX₃₆₁₋₃₇₄^{pSer367}; and (G) hDMX₃₃₅₋₃₇₃^{pSer342/pSer367} (peptides – concentration at 10x the K_d for each peptide – were passed over immobilized 14-3-3η, 25°C, 25 mM HEPES pH 7.5, 100 mM NaCl, 10 mM MgCl₂; experiments were performed in a multicycle kinetic format and data was fitted to a Langmuir model. K_d values were determined by fitting maximal response level at the end of injection against protein concentration using a steady state affinity model in the BIACORE evaluation software.

3-3η isoform is discussed below. hDMX₃₆₁₋₃₇₄^{pSer367} exhibited higher affinity ($K_d = 98.8 \pm 4.6$ nM) than hDMX₃₃₅₋₃₄₉^{pSer342} ($K_d = 20.0 \pm 1.2$ μM). hDM2 sequences bound with weaker affinity (hDM2₁₆₀₋₁₇₁^{pSer166} $K_d = 10.2 \pm 0.3$ μM and hDM2₁₈₀₋₁₉₂^{pSer186} $K_d = 31.6 \pm 1.9$ μM). As might be expected the highest affinity sequence (hDMX₃₆₁₋₃₇₄^{pSer367}) is a mode I 14-3-3 sequence/binder (see later) with Pro at the +2 position and Arg at the –3 position.

Because of its dimer structure, 14-3-3 is known to bind multiple binding partners simultaneously, either by binding two different phosphorylated residues from the same target or possibly two phosphorylated sites within a multiprotein complex [31,61–63]. Thus, doubly phosphorylated hDMX and hDM2 peptides were used to assess the effects of proximal phosphorylation on affinity. Two state binding in FA was observed for both doubly phosphorylated hDMX and hDM2 peptides

Table 2. K_d values for hDMX and hDM2 peptides binding to 14-3-3 proteins (in μM) (increasing affinity is denoted by increasingly darker grey shading).

Protein Peptide	14-3-3 η	14-3-3 β	14-3-3 τ	14-3-3 ζ	14-3-3 γ	14-3-3 σ	14-3-3 ϵ
hDMX ₃₃₅₋₃₄₉ ^{pSer342}	20.0 ± 1.2	49.4 ± 11.5	107.8 ± 6.0	95.8 ± 3.6	37.8 ± 0.7	135.9 ± 3.6	53.4 ± 2.9
hDMX ₃₆₁₋₃₇₄ ^{pSer367}	0.099 ± 0.005	0.51 ± 0.02	1.2 ± 0.2	0.92 ± 0.03	0.53 ± 0.04	3.6 ± 0.4	2.7 ± 0.2
hDMX ₃₃₅₋₃₇₃ ^{pSer342/pSer367} K_{d1}	0.030 ± 0.006	0.026 ± 0.009	–	–	0.091 ± 0.015	–	–
hDMX ₃₃₅₋₃₇₃ ^{pSer342/pSer367} K_{d2}	10.7 ± 1.2	7.6 ± 0.8	–	–	18.7 ± 0.7	–	–
hDM2 ₁₆₀₋₁₇₁ ^{pSer166}	10.2 ± 0.3	11.1 ± 0.5	29.3 ± 2.4	19.6 ± 0.2	3.9 ± 0.3	32.7 ± 1.4	23.0 ± 1.2
hDM2 ₁₈₀₋₁₉₂ ^{pSer186}	31.6 ± 1.9	207.9 ± 6.3	>250	165.8 ± 5.6	82.9 ± 2.1	>170	>260
hDM2 ₁₆₀₋₁₉₂ ^{pSer166/pSer186} K_{d1}	0.050 ± 0.012	–	–	–	0.089 ± 0.010	–	–
hDM2 ₁₆₀₋₁₉₂ ^{pSer166/pSer186} K_{d2}	17.5 ± 2.5	–	–	–	28.0 ± 0.8	–	–

(Fig. 2C for hDMX peptide and Fig. S4 for hDM2 peptide). Fitting for the observed biphasic-dose–response curves were performed in the same manner as for the short peptides by fitting each binding event separately to a 1 : 1 model (one peptide to one 14-3-3 monomer) so as to obtain stepwise K_d values. Accurate fitting was possible for 14-3-3 η , γ and β isoforms as reported in Table 2 (for 14-3-3 η , hDMX₃₃₅₋₃₇₃^{pSer342/pSer367} K_{d1} = 30.3 ± 6.4 nM and K_{d2} = 10.67 ± 1.2 μM , hDM2₁₆₀₋₁₉₂^{pSer166/pSer186}; K_{d1} = 49.6 ± 12.1 nM and K_{d2} = 17.5 ± 2.5 μM). Approximately 200-fold higher affinity K_{d1} was observed for hDM2₁₆₀₋₁₉₂^{pSer166/pSer186} compared to hDM2₁₆₀₋₁₇₁^{pSer166} whilst a more modest 3-fold increase in binding affinity for hDMX₃₃₅₋₃₇₃^{pSer342/pSer367} was observed in comparison to hDMX₃₆₁₋₃₇₄^{pSer367} (although enhancement was more pronounced for binding to β and γ isoforms).

Isothermal titration calorimetry was used as an orthogonal assay to confirm the binding affinities of hDMX and hDM2 peptides to 14-3-3 η and to gain additional information about the stoichiometry of the interactions. Moreover, such experiments provide thermodynamic data and as a label-free method require no immobilization/functionalization of any of the binding partners. Here data were obtained by titration of the peptide into 14-3-3 η protein (Fig. 2D,E and Fig. S7). Thermodynamic parameters for interaction of 14-3-3 with hDMX and hDM2 peptides obtained by ITC are summarized in Table 3.

Isothermal titration calorimetry data showed similar trends for binding of hDMX peptides to 14-3-3 η to those observed in the FA assays; binding affinities of hDMX₃₆₁₋₃₇₄^{pSer367}, hDMX₃₃₅₋₃₄₉^{pSer342} and hDMX₃₃₅₋₃₇₃^{pSer342/pSer367} were K_d = 870 ± 95 nM, K_d = 21 ± 3 μM and K_d = 14 ± 10 nM. An increase in binding affinity when both binding sites of hDM2 are present was also confirmed, with K_d = 151 ± 57 nM. The stoichiometry between doubly phosphorylated hDMX and hDM2 peptides and 14-3-3 η was found to be approximately 0.94 indicating a 1 : 1 binding model. If two phosphorylated sites from one peptide were binding simultaneously, the expected stoichiometry would be around 0.5. The contrasting absence of two binding events in the ITC data, when compared to the FA experiments, can be accounted for by the different experimental configurations. In the former, titration of the peptide into protein means that protein begins in excess and becomes saturated with the highest affinity site, whereas for FA, peptide begins in excess and protein (and therefore monomer/dimer ratio) varies in concentration across the experiment.

Finally, association and dissociation rates for the binding of hDMX and hDM2 peptides to 14-3-3 η were determined by SPR (Fig. 2E,F and Figs S8 and S9). Similar K_d values were confirmed from dose–response SPR. SPR measured affinities were broadly in agreement with K_d values determined from FA and ITC experiments (Table 2 and 3). For peptides exhibiting

Table 3. Thermodynamic parameters for hDMX(2) peptides/14-3-3 proteins.

	K_d (ITC)	ΔG (kJ·mol ⁻¹)	ΔH (kJ·mol ⁻¹)	$-T\Delta S$ (kJ·mol ⁻¹)	n	K_d (SPR) ^a	k_{on} (1/Ms)	k_{off} 1/s
hDMX ₃₃₅₋₃₄₉ ^{pSer342}	21 ± 3 μM	-26.7	-21.4 ± 1	-5.3	0.72	37 μM	–	–
hDMX ₃₆₁₋₃₇₄ ^{pSer367}	870 ± 95 nM	-34.6	-16.1 ± 0.2	-18.5	1.28	189 nM	3.89 × 10 ⁵	0.1208
hDMX ₃₃₅₋₃₇₃ ^{pSer342/pSer367}	14 ± 10 nM	-44.7	-22.1 ± 0.7	-22.6	0.94	8.6 nM	1.51 × 10 ⁶	0.0048
hDM2 ₁₆₀₋₁₉₂ ^{pSer166/pSer186}	151 ± 57 nM	-38.9	-12.3 ± 0.6	-26.6	0.94	155 nM	1.45 × 10 ⁶	0.1215

^aDose–response curves were fitted by plotting RUs against the peptide concentration.

lower affinities ($hDMX_{335-349}^{pSer342}$, $hDM2_{160-171}^{pSer166}$ and $hDM2_{180-192}^{pSer186}$) it was only possible to determine steady-state affinities, but not their kinetic profile (see [Supporting Information](#)). The doubly phosphorylated peptides showed the expected increase in affinity, which could be attributed to a much slower k_{off} rate in comparison to singly phosphorylated $hDMX_{361-374}^{pSer367}$ and $hDMX_{335-349}^{pSer342}$ peptides.

The 1 : 1 stoichiometry between the doubly phosphorylated peptides and 14-3-3 contrasts with previously reported work [61,62], although it may be that the length and/or accessible conformation of the $hDMX$ and $hDM2$ peptides are incompatible with the simultaneous engagement of both 14-3-3 protomers in the dimeric structure. To further explore this behaviour and understand the basis of cooperativity and affinity enhancement we performed additional experiments. To exclude the possible formation of higher-order oligomers (e.g. 14-3-3 tetramers held together by two peptides bridging two dimers), an analytical ultracentrifugation experiment was performed. The 14-3-3 η (at the concentration of 14 μ M, approximately corresponding to the second binding events observed in FA, Fig. 2C) and $hDMX_{335-373}^{pSer342/pSer367}$ peptide in two different concentration ratios (1 : 1 and 1 : 0.5, protein vs. peptide) were analysed. The sedimentation coefficient value remained unchanged for 14-3-3 protein alone and when varying peptide/protein concentrations, indicating that only one dimer of 14-3-3 η is involved in binding (see Fig. S10). Secondly, peptide length may also have a significant effect on the affinity and binding mode. This has been demonstrated in a recent study with p53 peptides with 14-3-3 σ , where

variation in the peptide length (from 9 to 32 residues) correlated with increased binding affinities [64]. Two long variants of $hDMX_{335-373}^{pSer342/pSer367}$ peptide were synthesized, with only one phosphorylation site: pSer367 or pSer342, extending the peptide length by 26 amino acids. The two peptides were tested in FA assays to decouple the influence of peptide length from the co-operative influence of having two phosphosites (Fig. 3). The $hDMX_{335-373}^{pSer342}$ peptide showed an increase in binding affinity with 14-3-3 η ($K_d = 5.4 \pm 1.1 \mu$ M) as expected, in comparison to the short version of the $hDMX_{335-349}^{pSer342}$ peptide ($K_d = 20.0 \pm 1.2 \mu$ M). On the other hand, increasing the peptide length for $hDMX_{335-373}^{pSer367}$ decreased the binding affinity ($K_d = 0.8 \pm 0.1 \mu$ M) and significantly lowered the maximum anisotropy signal. The lower maximum anisotropy signal observed might be due to the fluorophore being moved approximately 20 amino acids further from the binding pSer-367 (see earlier discussion on fluorophore mobility). Whilst there is a moderate increase in binding affinity of $hDMX_{335-373}^{pSer342}$ on increasing the peptide length this is insufficient for high-affinity interaction. Similarly, the slight loss in potency for the longer $hDMX_{335-373}^{pSer367}$ peptide relative to $hDMX_{361-374}^{pSer367}$ is noteworthy in considering the interaction with full-length protein as these data hint at interference from the additional residues, and is therefore likely to be important in relating these results to the behaviour for the full-length proteins. Taken together, the data indicate that proximal phosphorylation of both sites in $hDMX_{335-373}^{pSer342/pSer367}$ is required for high affinity 1 : 1 stoichiometric binding between $hDMX$ and

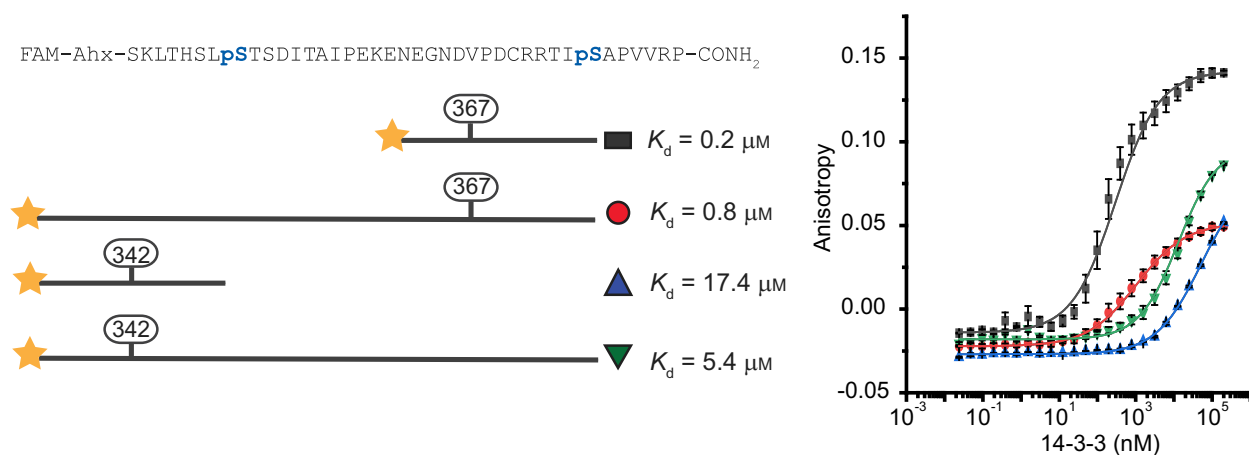


Fig. 3. Difference in the affinity between short $hDMX_{335-349}^{pSer342}$ and $hDMX_{361-374}^{pSer367}$ peptides and their longer singly phosphorylated variants ($hDMX_{335-373}^{pSer342}$ and $hDMX_{335-373}^{pSer367}$) as determined by fluorescence anisotropy titration (tracer 50 nM, 10 mM HEPES, 150 mM NaCl, 0.1% Tween 20, 0.1% BSA pH 7.4, concentration of proteins given as 14-3-3 monomer concentration, error bars represent SD for $n = 3$ replicates).

14-3-3 protomers. Given the absence of 1 : 2 binding, the presence of multiple sites may increase affinity through statistical rebinding or interaction with a second non-canonical phosphate-binding site on the surface of 14-3-3. The second binding event observed only in fluorescence anisotropy experiments, may represent a further non-specific binding event or an interaction linked to 14-3-3 dimerization [60] and will be investigated in future work.

Structural characterization of the interaction between 14-3-3 and hDMX or hDM2 peptides

The W-shaped structure of a 14-3-3 dimer provides a groove for phosphorylated client proteins to bind. One dimer usually accommodates two copies of phosphorylated sites from one target, but there are examples of two different targets simultaneously binding to one dimer of 14-3-3 proteins [61,62]. Phosphorylated Ser/Thr residues from partner proteins generally bind directly between Lys49 and Arg56 in helix α 3, and Arg127 and Tyr128 in helix α 5 as they form a basic binding pocket in otherwise acidic surroundings. Structural data were obtained by solving three crystal structures of hDMX₃₆₁₋₃₇₄^{pSer367} (PDB: 6YR5), hDM2₁₈₀₋₁₉₂^{pSer186} (PDB: 6YR6) and hDMX₃₃₅₋₃₇₃^{pSer342/pSer367} (PDB: 6YR7) in complex with 14-3-3 Δ C (the C-terminus was truncated for the crystallography purposes). Refinement statistics for all three structures are given in the ESI as are additional images of each structure with electron density for peptides in each monomer of 14-3-3 σ .

The hDMX₃₆₁₋₃₇₄^{pSer367}/14-3-3 σ structure was solved to a resolution of 2.25 Å with a dimer and two additional monomers of 14-3-3 σ (in green and blue) in the asymmetric unit, each binding a hDMX₃₆₁₋₃₇₄^{pSer367} peptide (cyan) in a conserved amphipathic groove (Fig. 4A and Fig S11 for additional images). Ten amino acids from hDMX₃₆₁₋₃₇₄^{pSer367} (RTI(pS)APVVRP) could be built into the electron density map. The phosphoserine of hDMX₃₆₁₋₃₇₄^{pSer367} is positioned in a basic pocket of 14-3-3 σ making polar contacts with Lys49, Arg56, Tyr119 and Arg129 (presented as dashed lines), whilst Asn226 makes polar contacts with the backbone of the peptide (Ile-1 with reference to pSer-367), in agreement with previously published 14-3-3 structures [38]. Additional polar contacts were found between Arg-3 of hDMX₃₆₁₋₃₇₄^{pSer367} and Glu182 of 14-3-3 σ , alongside Ala+1 and Thr+2 on the peptide backbone with Asn175 and Trp230 on the protein respectively. Hydrophobic contacts were found between Ile-1, Ala+1 and Pro+2 of the peptide with multiple residues on the protein (presented as spheres).

Structural evidence for the interaction of hDM2 with 14-3-3 proteins was obtained by solving the novel crystal structure of the hDM2₁₈₀₋₁₉₂^{pSer186} peptide in complex with 14-3-3 σ , to a resolution of 1.75 Å. The complex is crystallized in space group *P*1 with the asymmetric unit containing one dimer along with an additional two monomers of 14-3-3 σ (monomers A-D) with pSer186 peptide in each groove (in cyan). Six amino acids of the peptide were resolved in the electron density: RHK(pS)DS (Fig. 4B see Fig. S12 for additional images). pSer of the peptide is always located in the same position, between Lys49, Arg56, Arg129 and Tyr130 and the peptide is stabilized by polar contacts between Lys-1 and Asp225, His-2 and Glu182, Trp230, and the peptide backbone with Asn175 and Asn226. Arg-3 and Ser+2 peptide residues are also stabilized through hydrogen bonds with water molecules.

The structure of a doubly phosphorylated peptide hDMX₃₃₅₋₃₇₃^{pSer342/pSer367} in complex with 14-3-3 σ was solved to 2.1 Å resolution (Fig. 4C). Here, 14-3-3 σ crystallized as a dimer in space group C121 with the asymmetric unit containing one dimer (green) with additional electron density for the peptide (cyan) observed in both monomeric units of 14-3-3 σ (Fig. 4C and Fig. S13 for additional images). Based on previously published structures of doubly phosphorylated peptides, it was expected to observe pSer342 binding to monomer B and pSer367 binding to monomer A [31,61,65]. The electron density within the binding groove of monomer B could unambiguously be assigned to pSer342, whereby eight amino acids of the peptide could be resolved (HSL(pS)TSDI). The peptide was observed to adopt an unusual conformation by taking a sharp turn. A closer examination of the pSer342 binding site in monomer B of 14-3-3 σ shows pSer342 binding to a basic pocket as expected, making polar contacts with Arg56, Arg129 and Tyr130. In this orientation, the Ile+4 from the peptide makes hydrophobic contact with Leu218 and Ile219 on the protein (represented as spheres). Peptide residues Thr+1 and Ser+2 make polar contacts with Lys122, Asn175, Glu182 and Trp230, while Asn226 makes polar contacts with the backbone of the peptide. Overall, the C-terminus of the peptide takes a sharp turn after the pSer-Thr residues and this peptide conformation is stabilized by hydrogen bonds between water molecules and Thr+1, Ser+2 and Asp+3 peptide residues. In contrast, the electron density map within the binding groove of monomer A indicated partial ligand occupancy and could be interpreted in different ways, indicating an overlay of multiple conformations (both pSer342 and pSer367 sites, with the dominant electron

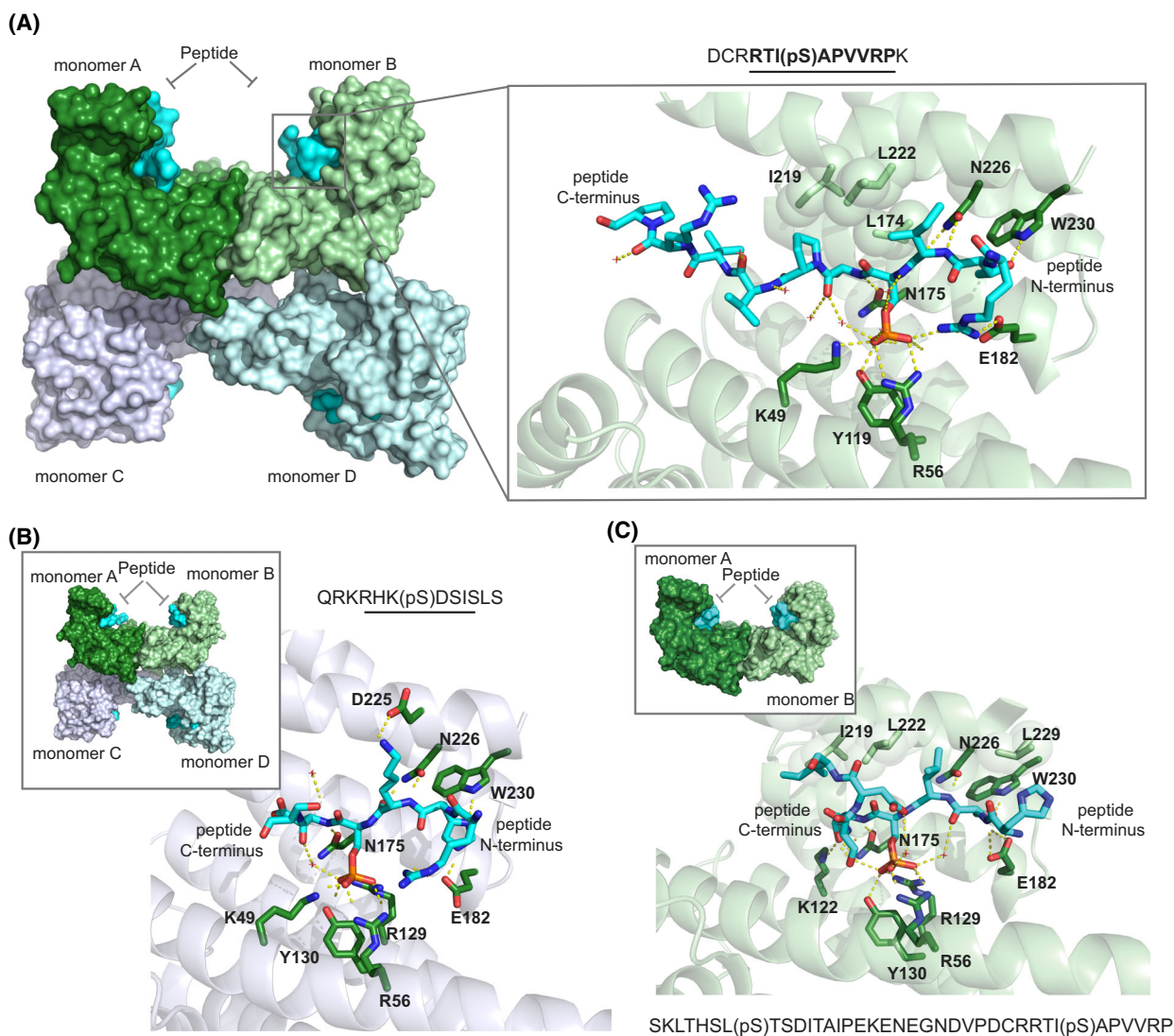


Fig. 4. Interactions between 14-3-3 and hDM peptides (A) $hDMX_{361-374}^{pSer367}/14-3-3$ structure (PDB: 6YR5); left hand side shows assembly of the $hDMX_{361-374}^{pSer367}/14-3-3$ complexes in the asymmetric unit with each singly phosphorylated peptide (cyan surface) bound to a 14-3-3 σ monomer (dark green, light green, light blue or light lilac surface), in its conserved amphipathic groove, right hand side shows monomer B (light green fold, 14-3-3 σ side chains shown as sticks with carbon dark green, nitrogen dark blue and oxygen red, $hDMX_{361-374}^{pSer367}$ shown as sticks, carbon in cyan, phosphorous orange, nitrogen and oxygen as above, non-covalent contacts shown as dashed lines) (B) $hDM2_{180-192}^{pSer186}/14-3-3$ (PDB: 6YR6) monomer C (light lilac fold, 14-3-3 σ and $hDM2_{180-192}^{pSer186}$ side chains shown as sticks with colour coding as above), inset shows complex in asymmetric unit (colour coding as above) (C) $hDMX_{335-373}^{pSer342/pSer367}/14-3-3$ structure (PDB: 6YR7) monomer B (light green fold, 14-3-3 σ and $hDMX_{335-373}^{pSer342/pSer367}$ side chains shown as sticks with colour coding as above), inset shows complex in asymmetric unit (colour coding as above). Structure images were generated using PYMOL 1.8 [69] and collated on an Adobe Illustrator CS6 artboard.

density map ascribable to pSer342 binding see Fig. S13 for additional images and discussion).

Discussion

We used FA, ITC and SPR to determine the binding affinity of $hDMX$ and $hDM2$ peptides to 14-3-3

proteins. $hDMX_{335-349}^{pSer342}$, $hDMX_{361-374}^{pSer367}$, $hDM2_{160-171}^{pSer166}$ and $hDM2_{180-192}^{pSer186}$ mimicking one phosphorylation site fit well to a 1 : 1 binding isotherm and exhibited greatest affinity towards the 14-3-3 η isoform, followed by γ , β , τ , ζ , σ and ϵ , respectively. The highest affinity peptide ($hDMX_{361-374}^{pSer367}$) bound strongly ($K_d = 98.8 \pm 4.6$ nM), whereas the

remaining sequences bound 14-3-3 less tightly (*hDMX*₃₃₅₋₃₄₉^{pSer342} $K_d = 20.0 \pm 1.2 \mu\text{M}$ {14-3-3 η isoform}, *hDM2*₁₆₀₋₁₇₁^{pSer166} $K_d = 10.2 \pm 0.3 \mu\text{M}$ and *hDM2*₁₈₀₋₁₉₂^{pSer186} $K_d = 31.6 \pm 1.9 \mu\text{M}$). Interestingly, different maximum anisotropies were observed for peptide binding across the 14-3-3 isoforms, which may reflect a difference in the 14-3-3 dimerization affinity [60] or mobility of the fluorophore. Binding experiments with doubly phosphorylated peptides were observed to result in two binding events. As expected for a multivalent interaction with 14-3-3 proteins [63], the first binding event in both cases was higher affinity than either monovalent interaction, whereas the second binding event was in the micromolar regime (for 14-3-3 η , *hDMX*₃₃₅₋₃₇₃^{pSer342/pSer367} $K_{d1} = 30.3 \pm 6.4 \text{ nM}$ and $K_{d2} = 10.67 \pm 1.2 \mu\text{M}$, *hDM2*₁₆₀₋₁₉₂^{pSer166/pSer186}, $K_{d1} = 49.6 \pm 12.1 \text{ nM}$ and $K_{d2} = 17.5 \pm 2.5 \mu\text{M}$). This enhancement in affinity for the first binding event was also observed in ITC experiments which lacked the second binding event (but were performed by titration of peptide into protein in contrast to the FA experiments) and SPR experiments which indicated that a slower k_{off} was associated with co-operative binding of doubly phosphorylated peptides. Importantly, for the doubly phosphorylated peptides, binding was negatively co-operative (i.e. less than additive; Table 4).

Taken together the data can be rationalized by assuming that the dimerization affinity of 14-3-3 differs across isoforms and occurs within the concentration regime of the FA experiments (Fig. 5). As the titration progresses, once 1 : 1 stoichiometry is attained, further addition of 14-3-3 results in unbound 14-3-3 monomer and eventually all peptides will be bound in complexes containing one peptide to two 14-3-3 monomers. For the doubly phosphorylated peptides early in the titration peptides bind with high

affinity in 1 : 1 stoichiometry – higher affinity likely results from statistical rebinding or a second phosphosite on the surface of the 14-3-3 protein. The second binding event either derives from a non-specific interaction, or arises from 14-3-3 dimerization [60] but is visible in the titration as a distinct binding event due to the strong affinity of the first event. Such behaviour is not observed in ITC experiments because the peptide is titrated into 14-3-3 protein so its concentration does not vary, and, the peptide becomes the saturating component. Considering the structural data for *hDMX*₃₆₁₋₃₇₄^{pSer367}, *hDM2*₁₈₀₋₁₉₂^{pSer186} and *hDMX*₃₃₅₋₃₇₃^{pSer342/pSer367} bind to 14-3-3 directly between K49 and R56 in helix α_3 , and R127 and Y128 in helix α_5 as is typical for 14-3-3 client proteins. The *hDMX*₃₆₁₋₃₇₄^{pSer367} peptide is a Mode I sequence (RXXpS/pTXP) which can account for its enhanced affinity in comparison to the other sequences [38,56]. Curiously, for the structure containing the longer *hDMX*₃₃₅₋₃₇₃^{pSer342/pSer367} peptide, the sequence surrounding pSer342 dominates in the electron density for bound ligand despite being the weaker 14-3-3 binding site of the two individual pSer sequences, this may favour the hypothesis of a second phosphorecognition site over the statistical rebinding model. Moreover, in the context of earlier cellular studies [26,41–45,48–53] the data highlight the complex nature by which phosphorylation regulates *hDMX* in particular [26,41–45]. pSer367 may be sufficient for 14-3-3 binding and the consequent effects on localization, stability and ultimately p53 function; the presence of both pSer342 and pSer367 confers some increase in 14-3-3 binding affinity (particularly for other isoforms), and it is plausible that accessibility of the binding sites in the full-length protein may play a crucial role that requires phosphorylation at both sites *in vivo*. In contrast, a much clearer difference in binding affinity for *hDM2*₁₆₀₋₁₉₂^{pSer166/pSer186} is observed in contrast to both monophosphorylated peptides and points to a functional requirement for double phosphorylation.

In conclusion, we have performed a biophysical and structural study on the interaction of 14-3-3 with peptides derived from *hDMX* and *hDM2*. We have shown that peptides derived from *hDMX* containing pSer342 or pSer367 and from *hDM2* containing pSer166 or pSer186 exhibit affinity for 14-3-3 as demonstrated by FA, ITC and SPR. Structural analyses reveal that the peptides bind to 14-3-3 directly between K49 and R56 in helix α_3 , and R127 and Y128 in helix α_5 as is typical for 14-3-3 client proteins. For high-affinity binding, proximal phosphosites are beneficial and in the case of *hDM2* essential. In contrast to other doubly phosphorylated peptides of this length the interaction involves one

Table 4. Thermodynamic values for binding of *hDM2* and *hDMX* peptides to 14-3-3 η .

Peptide	$\Delta G_{14-3-3\eta}$ (kJ·mol ⁻¹) ^a	$\Delta G_{14-3-3\eta}$ (kJ·mol ⁻¹) ^b
<i>hDMX</i> ₃₃₅₋₃₄₉ ^{pSer342}	-21.1	-26.7
<i>hDMX</i> ₃₆₁₋₃₇₄ ^{pSer367}	-34.3	-34.6
<i>hDMX</i> ₃₃₅₋₃₇₃ ^{pSer342/pSer367}	-37.2	-44.7
<i>hDM2</i> ₁₆₀₋₁₇₁ ^{pSer166}	-22.8	n.d
<i>hDM2</i> ₁₈₀₋₁₉₂ ^{pSer186}	-20.0	n.d
<i>hDM2</i> ₁₆₀₋₁₉₂ ^{pSer166/pSer186}	-36.0	38.9

^aCalculated from K_d values determined by fluorescence anisotropy titration of FAM-Ahx labelled peptides with 14-3-3 η ; ^bDetermined by ITC for Acetyl labelled peptides titration with 14-3-3 η .

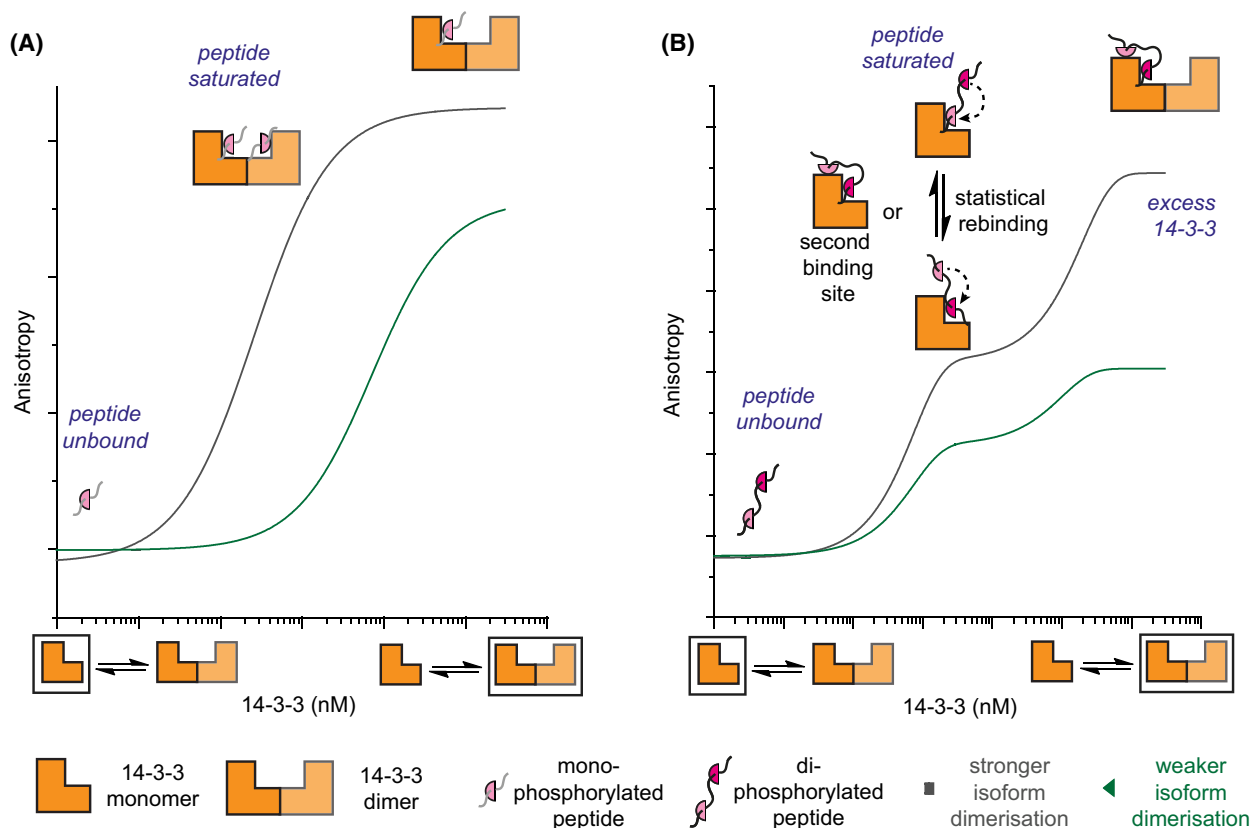


Fig. 5. Schematic overview depicting equilibrium behaviour and potential hypotheses for isoform dependent differences in anisotropies linked to 14-3-3 dimerization alongside reasons for the enhanced affinity of doubly phosphorylated peptides.

peptide for each 14-3-3 protomer [61–63]. The additional affinity likely derives from a reduced k_{off} rate for doubly phosphorylated peptides. Importantly, the results suggest that sequential phosphorylation of proximal sites in both *hDMX* and *hDM2* plays a role in promoting changes in their localization and degradation in a cellular context. Thus, these data provide structural insight on the indirect effects of 14-3-3 on the p53 pathway, which may inform the development of chemical intervention strategies (e.g. use of kinase inhibitors) and provide starting points for structure-based ligand design of 14-3-3/*hDMX* and 14-3-3/*hDM2* modulators, both stabilizers and inhibitors.

Materials and methods

Peptide synthesis

General remarks

Resins and amino acids were purchased from either Sigma–Aldrich (part of Merck Life Science UK Limited, Gillingham, Dorset, UK) or Novabiochem (part of Merck Life Science UK Limited, Gillingham, Dorset, UK). All amino acids were

N-Fmoc protected and side chains protected with Boc (His, Lys), *t*-Bu (Asp, Glu, Ser, Thr), Pbf (Arg), Trt (Asn, Gln). Peptides were synthesized either manually or using a microwave-assisted automated peptide synthesizer (CEM Liberty Blue) on a 0.05 or 0.1 mmol scale. DMF used in peptide synthesis was of ACS grade and from Sigma–Aldrich.

Manual peptide synthesis

Manual peptide synthesis followed this cycle: swelling of a resin (20 min) in cartridge used for solid-phase synthesis, washing (DMF, $3 \times 2 \text{ mL} \times 2 \text{ min}$), deprotection (Method A), and coupling of the desired amino acid (Method B), where successful coupling and deprotection were determined by a colour test (Method C). Acetylation (Method D) or coupling of a fluorescent dye (Method E) were performed prior to cleavage (Method F).

Method A: Deprotection N-terminal Fmoc-protecting groups were removed by adding 20% piperidine in DMF ($5 \times 2 \text{ mL} \times 2 \text{ min}$) and washed with DMF ($5 \times 2 \text{ mL} \times 2 \text{ min}$) after.

Method B: Manual coupling of amino acid and Ahx.

The desired amino acid or Ahx (5 equiv.), DIPEA (10 equiv.) and HCTU (5 equiv.) were dissolved in DMF

(2 mL) and added to the resin, followed by agitation for 1 h. Reagents were removed by filtration and the resin was washed with DMF (3 × 2 mL × 2 min).

Method C: Kaiser test.

Successful coupling or deprotection for any residue coupled manually was determined by the Kaiser test. A few resin beads were transferred into a vial and mixed with 2 drops of each of the solutions:

- 1 Ninhydrin (5% w/v) in ethanol,
- 2 Phenol (80% w/v) in ethanol,
- 3 1 mM KCN (aq.) in pyridine (2% v/v).

The solution was heated at 100 °C for 5 min before observing the change in colour. Successful deprotection was observed by colour of the beads changing into blue, where successful coupling gave no change in colour.

Method D: N-terminal acetylation.

Acetic anhydride (10 equiv.) and DIPEA (10 equiv.) were dissolved in DMF (2 mL) and the solution was transferred to the resin. After 2 h, the resin was drained and washed with DMF (3 × 2 mL × 2 min). Successful capping was determined by colour test (Method C).

Method E: N-terminal Fluorescent Dye coupling.

5,6-carboxyfluorescein (5 equiv.), DIPEA (5 equiv.) and HCTU (5 equiv.) were dissolved in DMF (2 mL) and added to the resin, followed by agitation for 1 h. Reagents were filtered and the resin was washed with DMF (3 × 2 mL × 2 min) ahead of cleavage and deprotection.

Method F: Cleavage and deprotection of peptides of the resin.

After elongation and acetylation or fluorescent dye coupling were complete, the resin was washed with CH₂Cl₂ (5 × 2 × 2 min), Et₂O (5 × 2 mL × 2 min) and dried under vacuum. Peptides were cleaved and side-chain deprotected using 'Reagent K' TFA : EDT : Thioanisole : Phenol : H₂O 82 : 3 : 5 : 5 : 5 (2 mL × 3 h). The peptide was precipitated in ice-cold Et₂O (10 mL) and placed in a centrifuge (1107 g × 5 min). The supernatant was removed, the precipitate resuspended in ice-cold Et₂O and placed in a centrifuge again (3×). The precipitate was dried under a stream of nitrogen overnight, before being dissolved in H₂O and lyophilized.

Automated peptide synthesis method

Peptides prepared using automated peptide synthesizer followed cycles described below. Resin loading cycle cleans the reaction vessel, washes with DMF : DCM (1 : 1), transfers resin to the reaction vessel, washes with DMF : DCM (1 : 1), and drains the vessel at the end of a cycle. Deprotection and coupling cycle consists of: washing with DMF (4 mL), adding 20% piperidine in DMF (6 mL), microwave deprotection cycle (30 s), washing with DMF (4 + 4 + 4 + 4 mL), the addition of amino acid (2.5 mL, 5 eq or 3 eq for phosphorylated amino acids), coupling reagent (1 mL, 5 eq) and

activator base (0.5 mL, 5 eq), coupling microwave cycle (5 min), washing with DMF (2 mL) and draining. HCTU and DIPEA were used during automated peptide synthesis as well. As a rule, all amino acids were coupled using 75 °C coupling and deprotection cycles up to Ser(PO(OBzl)OH)-OH or Thr(PO(OBzl)OH)-OH, where conventional coupling and deprotection method was used (coupling at the rt for 2 h, deprotection at rt for 15 min) as well for every amino acid following pSer/pThr. After the final residue was coupled, the resin was ejected from the reaction vessel. Ahx coupling, deprotection, acetylation or fluorescent dye coupling, and cleavage were performed manually using the methods described above.

Peptide purification

Crude peptides were dissolved in H₂O or DMSO and purified by UV- or MS-directed HPLC. Jupiter Proteo (250 × 21.2 mm) or a Kinetex EVO C18 (250 × 21.2 mm) preparative column (reversed-phase) was used with an increasing gradient of acetonitrile in water with 0.1% formic acid, over 30 min at the flow rate of 10 mL·min⁻¹. Fractions containing peptides were combined, concentrated and lyophilized. The purity of peptides was assessed by analytical HPLC and HRMS.

Protein expression and purification

The pProEx HTb-His-14-3-3 constructs were expressed in BL21(DE3) cells. A single colony from a freshly made agar plate (8 g LB broth mixed with 8 g agar in 400 mL, autoclaved and poured into Petri dishes to use for the transformation of plasmids) was picked and mixed with 5 mL of LB media with ampicillin to inoculate a starter culture overnight at 37 °C. The cells were grown in 2 L of TB media (48 g peptone, 24 g yeast, 4.6 g KH₂PO₄, 24 g KHPO₄, 5 mL glycerol in 2 L of dH₂O, autoclaved for 20 min at 121 °C) at 37 °C until the OD reached 0.4–0.6. Expression was induced by adding 0.4 mM IPTG and agitating overnight at 18 °C. The expression culture was spun down (7871 g, 20 min, 4 °C), resuspended in 200 mL of lysis buffer (50 mM Tris, 300 mM NaCl, 12.5 mM imidazole, 2 mM β-mercaptoethanol) with 5 mM MgCl₂ and DNase (1 : 1000). The cells were lysed by French press or sonication and the solid fragments were removed by centrifugation (49 192 g, 30 min, 4 °C). The cleared lysate was loaded on a Ni²⁺-NTA column, washed with 50 mM Tris, 300 mM NaCl, 12.5 mM imidazole, 2 mM β-mercaptoethanol, 0.1% triton X-100, and the protein was eluted with 50 mM Tris, 300 mM NaCl, 250 mM imidazole and 2 mM β-mercaptoethanol. Imidazole was removed by overnight dialysis using the Tris buffer (50 mM Tris, 300 mM NaCl, 2 mM β-mercaptoethanol), full-length proteins were concentrated by centrifugation, rebuffed in HEPES buffer (25 mM HEPES pH 7.5, 100 mM NaCl, 10 mM MgCl₂ and 0.5 mM TCEF) and stored in –80 °C

freezer. ΔC proteins were dialyzed with TEV protease to remove the expression tag and purified again on Ni²⁺-NTA column, followed by size-exclusion chromatography (HiLoad 16/600 Superdex 75 pg column) in HEPES buffer (20 mM HEPES, 150 mM NaCl, 2 mM DTT). ΔC proteins were concentrated and rebuffed for -80°C storage. All proteins were analyzed by ESI QTOF-MS.

Fluorescence anisotropy

Direct titration assay

All assays were performed in 384 well plates (each experiment was run in triplicates) and data were collected by Perkin Elmer EnVision 2013 plate reader with excitation at 480 nm (30 nm bandwidth), polarised dichroic mirror at 505 nm and emission at 535 nm (40 nm bandwidth, S and P polarised). Experiments were carried out in HBS buffer (10 mM HEPES, 150 mM NaCl, pH 7.4) + 0.1% Tween 20 + 0.1% BSA). A $\frac{1}{2}$ fold dilution series was performed in the titration, with plates read after 30 min, 4 h and 20–24 h. These gave consistent data and values when fitted. Collected data were processed in Microsoft Excel using the equations below. Total intensity I and anisotropy r were calculated using Equations 1 and 2 for each well. Average anisotropy was plotted against protein concentration using OriginPro and a logistic curve was fitted to give r_{\min} and r_{\max} . Using Equation 3 anisotropy was converted into fraction bound and multiplied by peptide concentration to be fitted in Origin using Equation 5 to obtain K_d values.

$$I = 2PG + S \quad (1)$$

$$r = \frac{S - PG}{I} \quad (2)$$

$$L_b = \frac{(r - r_{\min})}{\lambda(r_{\max} - r) + r - r_{\min}} \quad (3)$$

$$y = r_{\min} + \frac{r_{\max} - r_{\min}}{1 + 10^{(x - \log x_0)}} \quad (4)$$

$$y = \frac{((K + X + FL) - \sqrt{((K + X + FL)^2 - 4xFL))}}{2} \quad (5)$$

r = anisotropy, I = total intensity, P = perpendicular intensity, S = parallel intensity, L_b = fraction ligand bound, $\lambda = I_{\text{bound}}/I_{\text{unbound}} = 1$, FL = fluorescent ligand concentration, $K = K_d$.

Surface plasmon resonance

Experiments were performed at 25°C using a Biacore T200 instrument (GE Healthcare, Buckinghamshire, UK). For

immobilization, the running buffer was HBS buffer (HEPES, NaCl, Tween-20, pH 7.4). 14-3-3 η was immobilized on an NTA sensor chip (Series S Sensor Chip GE Healthcare) using NTA reagent and Biacore Amine Coupling Kit. Briefly, 14-3-3 η was diluted to $0.2 \text{ mg}\cdot\text{mL}^{-1}$ and $200 \mu\text{L}$ was injected over a chip surface that had been activated with an injection of Ni²⁺, followed by $140 \mu\text{L}$ of 1 : 1 NHS/EDC. A $30 \mu\text{L}$ of 0.5 M ethanolamine was then injected to cap the excess free amine groups. Immobilization levels of the 14-3-3 η were found to be around 2000 response units (RU) for kinetic measurements. *hDMX* and *hDM2* peptides were serially diluted 11 times from concentrations 10 times the K_d values measured in FA, on a 96-well plate. Then, $20 \mu\text{L}$ of these solutions were injected over a 14-3-3 η immobilized surface for 1 min at the $20 \text{ mL}\cdot\text{min}^{-1}$ flow rate, followed by a 4 min regeneration period with HBS buffer. Kinetics and the binding affinity were calculated using the BIACORE evaluation software (Buckinghamshire, UK). Standard dose–response curves were fitted by plotting RUs against the peptide concentration.

Isothermal titration calorimetry

Isothermal titration calorimetry experiments were carried out on a MicroCal iTC200 in HBS buffer at 25°C (25 mM HEPES pH 7.5, 100 mM NaCl, 10 mM MgCl₂, 0.5 mM TCEP). Peptides (0.2–1 M) in the syringe were titrated into a cell containing 14-3-3 η (0.02 or 0.1 M). Data were fitted using MICROCAL software (Northampton, MA, USA) to give binding constant (K_d), enthalpy (ΔH), entropy (ΔS) and binding stoichiometry (n).

Protein crystallography

A solution of $14 \text{ mg}\cdot\text{mL}^{-1}$ 14-3-3 $\sigma\Delta C$ with *hDMX*₃₆₁₋₃₇₄^{pSer367} peptide in 1 : 2 molar ratio was incubated overnight in crystallization buffer (20 mM HEPES pH 7.5, 2 mM MgCl₂ and 2 mM BME). Crystals were obtained at 4°C in a hanging drop vapour diffusion set up with 0.2 M sodium sulfate, 0.1 M Bis-Tris propane, 20% w/v PEG 3350 at pH 8.5 as precipitation buffer. Protein/peptide solution and precipitation buffer were mixed in a 1 : 1 ratio in a total volume of $2 \mu\text{L}$. Diffraction data were recorded at the DESY, Petra III P11, Hamburg to a resolution of 2.2 \AA . *hDMX*₃₃₅₋₃₇₄^{pSer342/pSer367} crystals were obtained at 4°C after overnight incubation of $12 \text{ mg}\cdot\text{mL}^{-1}$ 14-3-3 $\sigma\Delta C$ with *hDMX*₃₃₅₋₃₇₄^{pSer342/pSer367} peptide (1 : 2 ratio) in sodium citrate dihydrate, bis-tris propane, pH 8, 20% PEG 3350. *hDM2*₁₈₀₋₁₉₂^{pSer186} crystals were obtained at 4°C after overnight incubation of $12 \text{ mg}\cdot\text{mL}^{-1}$ 14-3-3 $\sigma\Delta C$ with *hDM2*₁₈₀₋₁₉₂^{pSer186} (1 : 2 ratio) in 0.0375 M CdSO₄ H₂O, 0.075 M HEPES, pH 7.5, 0.75 M NaAc 3H₂O and 25% glycerol. Diffraction data for *hDMX*₃₃₅₋₃₇₄^{pSer342/pSer367} and *hDM2*₁₈₀₋₁₉₂^{pSer186} crystals were recorded at the Diamond Light source, UK with a resolution of 2.1 \AA for *hDMX*₃₃₅₋₃₇₄^{pSer342/pSer367} and a resolution of 1.75 \AA for *hDM2*₁₈₀₋₁₉₂^{pSer186}. The CCP4 software package [66] was used for

structure determination by molecular replacement with 4DAT (PDB accession code) as a template for the 14-3-3 σ structure. Further rounds of manual model building and refinement were performed using COOT [67] and REFMAC [68] respectively. Data collection and refinement statistics for each structure are provided in Table 5.

Analytical ultracentrifugation

AUC-SV experiments were performed using a Beckman Coulter Optima XL-I ultracentrifuge. Samples were prepared in HBS buffer (10 mM HEPES, 150 mM NaCl, pH 7.4) and loaded into 12 mm aluminium centrepieces with sapphire windows. Three samples were run: (I) 14 μ M 14-3-3 η , (II) 14 μ M 14-3-3 η + 7 μ M hDMX₃₃₅₋₃₇₄^{pSer342/pSer367}

and (III) 14 μ M 14-3-3 η + 14 μ M hDMX₃₃₅₋₃₇₄^{pSer342/pSer367}, with buffer as a reference, and recorded at 206 070 g in the An50-Ti rotor, at the 25 °C. The diffusion-deconvoluted sedimentation coefficient distributions $c(s)$ were calculated using the SEDFIT program (Bethesda, MD, USA).

Circular dichroism spectroscopy

Spectra were recorded on a Chirascan circular dichroism spectropolarimeter (Applied Photophysics, Leatherhead, UK), using 1 mm cells, scan speed of 5 nm·min⁻¹, 2 nm bandwidth and 180–260 nm range. The experiments were performed in 50 mM sodium phosphate buffer, pH 7.5 at 20 °C. The spectra were averaged over three repeats with

Table 5. Data collection and refinement statistics. Values in parenthesis correlate to high-resolution shell if not indicated otherwise.

	hDMX ₃₆₁₋₃₇₄ ^{pSer367}	hDMX ₃₄₅₋₃₇₄ ^{pSer342/pSer367}	hDM2 ₁₈₀₋₁₉₂ ^{pSer186}
PDB ID	6YR5	6YR7	6YR6
Source	DESY, PETRA III	DLS	DLS
Beamline	P11	I03	I03
Wavelength	1.033208	0.9763	0.9763
Resolution (Å)	74.53–2.25	45.77–2.11	73.26–1.75
Space group	P 1	C 1 2 1	P 1
Cell constants a,b,c, α , β , γ	63.95 Å 75.30 Å 78.39 Å 95.15° 113.14° 93.84°	133.11 Å 70.21 Å 80.63 Å 90.00° 101.97° 90.00°	63.23 Å 74.57 Å 77.97 Å 98.43° 111.09° 93.12°
% Data completeness (in resolution range)	97.3 (74.53–2.10) 97.6 (71.50–2.25)	99.1 (56.26–2.10) 91.2 (65.11–2.10)	94.9 (56.90–1.75) 90.0 (73.26–1.75)
Total reflections	438 829 (26 508)	83 977 (7971)	445 180 (21 904)
Unique reflections	75 667 (4474)	42 037 (3995)	127 733 (12 631)
Redundancy	5.8 (5.9)	2.0 (2.0)	3.5 (3.5)
R_{merge}	0.11	0.04	0.07
$\langle I/\sigma(I) \rangle$	5.3 (at 2.25 Å)	0.68 (at 2.10 Å)	1.33 (at 1.75 Å)
Refinement statistics			
Resolution range (Å)	74.53–2.25 (2.33–2.25)	45.77–2.11 (2.19–2.11)	56.90–1.75 (1.81–1.75)
Wilson B-factor (Å ²)	27.3	35.8	25.3
Anisotropy	0.338	0.397	0.241
Bulk solvent $k_{\text{sol}}(\text{e}/\text{Å}^3)$, $B_{\text{sol}}(\text{Å}^2)$	0.30, 31.7	0.36, 40.0	0.41, 47.8
L-test for twinning	$\langle I \rangle = 0.47$, $\langle L2 \rangle = 0.30$	$\langle I \rangle = 0.50$, $\langle L2 \rangle = 0.34$	$\langle I \rangle = 0.50$, $\langle L2 \rangle = 0.33$
Estimated twinning fraction	No twinning to report.	No twinning to report.	No twinning to report.
Fo, Fc correlation	0.93	0.94	0.94
Total number of atoms	7709	7376	15129
Average B, all atoms (Å ²)	34.0	54.0	40.0
R factor (%)	19.71 (28.03)	21.56 (34.09)	19.89 (28.06)
R_{free} (%)	21.94 (30.14)	25.00 (34.57)	22.38 (29.45)
R_{free} test set	2993 reflections (4.85%)	2108 reflections (5.02%)	6318 reflections (5.03%)
No. of protein non-H atoms	7709	3848	8038
No. of macromolecules non-H atoms	7333	3650	7296
No. of ligand non-H atoms	5	45	101
No. of water molecules	371	179	693
R.m.s.d bond lengths (Å)	0.017	0.004	0.005
R.m.s.d bond angles (°)	1.95	0.86	0.93
Ramachandran plot			
Favoured region (%)	97.68	98.23	98.45
Outliers (%)	0.22	0	0

a buffer baseline subtracted. Protein concentrations of approximately $0.2 \text{ mg}\cdot\text{mL}^{-1}$ were used for all proteins.

Acknowledgements

We would like to thank Dr Iain Manfield for his support with ITC and SPR measurements and Gavin O'Mahony, AstraZeneca for ongoing collaboration and useful discussions. This work was supported by EPSRC (EP/N013573/1 and EP/KO39292/1). This project has received funding from the European Union's Horizon 2020 research and innovation programme under the Marie Skłodowska-Curie programme H2020-MSCA-ITN-2015 grant number 675179 (The TASPPi project). This work was supported by Diamond beam time awarded under proposal number MX19248. AJW wishes to acknowledge the support of a Royal Society Leverhulme Trust Senior Fellowship (SRF\R1\191087)

Conflict of interest

CO is co-founder and shareholder of Ambagon Therapeutics. The authors declare no competing financial interests.

Peer Review

The peer review history for this article is available at <https://publons.com/publon/10.1111/febs.16433>.

Data availability statement

The data that supports the findings of this study are available in [Figs 1–4] and the [Supporting Information](#) of this article. The structural data that support these findings are openly available in the wwPDB at <https://doi.org/10.2210/pdb6YR5/pdb>, <https://doi.org/10.2210/pdb6YR7/pdb> and <https://doi.org/10.2210/pdb6YR6/pdb>.

Author contributions

SS, CO, SLW and AJW conceived and designed the research program, SS designed studies and performed the research with support from MW, CT and CO on crystallographic analyses. The manuscript was written by SS and AJW and edited into its final form by SLW and AJW with contributions from all authors.

References

- Hafner A, Bulyk ML, Jambhekar A, Lahav G. The multiple mechanisms that regulate p53 activity and cell fate. *Nat Rev Mol Cell Biol.* 2019;**20**:199–210.
- Hoe KK, Verma CS, Lane DP. Drugging the p53 pathway: understanding the route to clinical efficacy. *Nat Rev Drug Discov.* 2014;**13**:217–36.
- Khoury K, Popowicz GM, Holak TA, Domling A. The p53-MDM2/MDMX axis – a chemotype perspective. *MedChemComm.* 2011;**2**:246–60.
- Zhao Y, Aguilar A, Bernard D, Wang S. Small-molecule inhibitors of the MDM2–p53 protein-protein interaction (MDM2 inhibitors) in clinical trials for cancer treatment. *J Med Chem.* 2015;**58**:1038–52.
- Liu Y, Wang X, Wang G, Yang Y, Yuan Y, Ouyang L. The past, present and future of potential small-molecule drugs targeting p53-MDM2/MDMX for cancer therapy. *Eur J Med Chem.* 2019;**176**:92–104.
- Wade M, Wang YV, Wahl GM. The p53 orchestra: Mdm2 and Mdmx set the tone. *Trends Cell Biol.* 2010;**20**:299–309.
- Wade M, Li Y-C, Wahl GM. MDM2, MDMX and p53 in oncogenesis and cancer therapy. *Nat Rev Cancer.* 2013;**13**:83.
- Shadfan M, Lopez-Pajares V, Yuan Z-M. MDM2 and MDMX: alone and together in regulation of p53. *Transl Cancer Res.* 2012;**1**:88–99.
- Momand J, Zambetti GP, Olson DC, George D, Levine AJ. The mdm-2 oncogene product forms a complex with the p53 protein and inhibits p53-mediated transactivation. *Cell.* 1992;**69**:1237–45.
- Shvarts A, Steegenga WT, Riteco N, van Laar T, Dekker P, Bazuine M, et al. MDMX: a novel p53-binding protein with some functional properties of MDM2. *EMBO J.* 1996;**15**:5349–57.
- Popowicz G, Czarna A, Holak T. Structure of the human Mdmx protein bound to the p53 tumor suppressor transactivation domain. *Cell Cycle.* 2008;**7**:2441–3.
- Kussie PH, Gorina S, Marechal V, Elenbaas B, Moreau J, Levine AJ, et al. Structure of the MDM2 oncoprotein bound to the p53 tumor suppressor transactivation domain. *Science.* 1996;**274**:948–53.
- Karni-Schmidt O, Lokshin M, Prives C. The roles of MDM2 and MDMX in cancer. *Annu Rev Pathol Mech Dis.* 2016;**11**:617–44.
- Honda R, Tanaka H, Yasuda H. Oncoprotein MDM2 is a ubiquitin ligase E3 for tumor suppressor p53. *FEBS Lett.* 1997;**420**:25–7.
- Haupt Y, Maya R, Kazaz A, Oren M. Mdm2 promotes the rapid degradation of p53. *Nature.* 1997;**387**:296–9.
- Linares LK, Hengstermann A, Ciechanover A, Müller S, Scheffner M. HdmX stimulates Hdm2-mediated ubiquitination and degradation of p53. *Proc Natl Acad Sci USA.* 2003;**100**:12009–14.
- Nomura K, Klejnot M, Kowalczyk D, Hock AK, Sibbet GJ, Vousden KH, et al. Structural analysis of MDM2 RING separates degradation from regulation of p53 transcription activity. *Nat Struct Mol Biol.* 2017;**24**:578–87.

- 18 Linke K, Mace PD, Smith CA, Vaux DL, Silke J, Day CL. Structure of the MDM2/MDMX RING domain heterodimer reveals dimerization is required for their ubiquitylation in trans. *Cell Death Differ.* 2008;**15**:841–8.
- 19 Tackmann NR, Zhang Y. Mouse modelling of the MDM2/MDMX–p53 signalling axis. *J Mol Cell Biol.* 2017;**9**:34–44.
- 20 Wang W, Qin J-J, Rajaei M, Li X, Yu X, Hunt C, et al. Targeting MDM2 for novel molecular therapy: beyond oncology. *Med Res Rev.* 2020;**40**:856–80.
- 21 Falcicchio M, Ward JA, Macip S, Doveston RG. Regulation of p53 by the 14-3-3 protein interaction network: new opportunities for drug discovery in cancer. *Cell Death Discov.* 2020;**6**:126.
- 22 de Polo A, Vivekanandan V, Little JB, Yuan Z-M. MDMX under stress: the MDMX-MDM2 complex as stress signals hub. *Transl Cancer Res.* 2016;**5**:725–32.
- 23 Waning DL, Lehman JA, Batuello CN, Mayo LD. Controlling the Mdm2-Mdmx-p53 circuit. *Pharmaceuticals.* 2010;**3**:1576–93.
- 24 Zuckerman V, Lenos K, Popowicz GM, Silberman I, Grossman T, Marine J-C, et al. c-Abl phosphorylates hdmx and regulates its interaction with p53*. *J Biol Chem.* 2009;**284**:4031–9.
- 25 Shieh S-Y, Ikeda M, Taya Y, Prives C. DNA damage-induced phosphorylation of p53 alleviates inhibition by MDM2. *Cell.* 1997;**91**:325–34.
- 26 LeBron C, Chen L, Gilkes DM, Chen J. Regulation of MDMX nuclear import and degradation by Chk2 and 14-3-3. *EMBO J.* 2006;**25**:1196–206.
- 27 Aitken A. 14-3-3 proteins: a historic overview. *Semin Cancer Biol.* 2006;**16**:162–72.
- 28 Aghazadeh Y, Papadopoulos V. The role of the 14-3-3 protein family in health, disease, and drug development. *Drug Discov Today.* 2016;**21**:278–87.
- 29 Fan X, Cui L, Zeng Y, Song W, Gaur U, Yang M. 14-3-3 proteins are on the crossroads of cancer, aging, and age-related neurodegenerative disease. *Int J Mol Sci.* 2019;**20**:3518.
- 30 Joo Y, Schumacher B, Landrieu I, Bartel M, Smet-Nocca C, Jang A, et al. Involvement of 14-3-3 in tubulin instability and impaired axon development is mediated by Tau. *FASEB J.* 2015;**29**:4133–44.
- 31 Stevers LM, Lam CV, Leysen SFR, Meijer FA, van Scheppingen DS, de Vries RMJM, et al. Characterization and small-molecule stabilization of the multisite tandem binding between 14-3-3 and the R domain of CFTR. *Proc Natl Acad Sci USA.* 2016;**113**:E1152–61.
- 32 Wolter M, de Vink P, Neves JF, Srdanovic S, Higuchi Y, Kato N, et al. Selectivity via cooperativity: preferential stabilization of the p65/14-3-3 interaction with semi-synthetic natural products. *J Am Chem Soc.* 2020;**142**:11772–83.
- 33 Kondo Y, Ognjenović J, Banerjee S, Karandur D, Merk A, Kulhanek K, et al. Cryo-EM structure of a dimeric B-Raf:14-3-3 complex reveals asymmetry in the active sites of B-Raf kinases. *Science.* 2019;**366**:109–15.
- 34 Stevers LM, Sijbesma E, Botta M, MacKintosh C, Obsil T, Landrieu I, et al. Modulators of 14-3-3 protein-protein interactions. *J Med Chem.* 2018;**61**:3755–78.
- 35 Madeira F, Park YM, Lee J, Buso N, Gur T, Madhusoodanan N, et al. The EMBL-EBI search and sequence analysis tools APIs in 2019. *Nucleic Acids Res.* 2019;**47**:W636–41.
- 36 Gogl G, Tugaeva KV, Eberling P, Kostmann C, Trave G, Sluchanko NN. Hierarchized phosphotarget binding by the seven human 14-3-3 isoforms. *Nat Commun.* 2021;**12**:1677.
- 37 Sengupta A, Liriano J, Bienkiewicz EA, Miller BG, Frederick JH. Probing the 14-3-3 isoform-specificity profile of protein-protein interactions stabilized by fusicoccin A. *ACS Omega.* 2020;**5**:25029–35.
- 38 Obsil T, Obsilova V. Structural basis of 14-3-3 protein functions. *Semin Cell Dev Biol.* 2011;**22**:663–72.
- 39 Benzinger A, Popowicz GM, Joy JK, Majumdar S, Holak TA, Hermeking H. The crystal structure of the non-liganded 14-3-3 σ protein: insights into determinants of isoform specific ligand binding and dimerization. *Cell Res.* 2005;**15**:219–27.
- 40 Gardino AK, Smerdon SJ, Yaffe MB. Structural determinants of 14-3-3 binding specificities and regulation of subcellular localization of 14-3-3-ligand complexes: a comparison of the X-ray crystal structures of all human 14-3-3 isoforms. *Semin Cancer Biol.* 2006;**16**:173–82.
- 41 Lopez-Pajares V, Kim MM, Yuan Z-M. Phosphorylation of MDMX mediated by Akt leads to stabilization and induces 14-3-3 binding *. *J Biol Chem.* 2008;**283**:13707–13.
- 42 Jin Y, Dai M-S, Lu SZ, Xu Y, Luo Z, Zhao Y, et al. 14-3-3 γ binds to MDMX that is phosphorylated by UV-activated Chk1, resulting in p53 activation. *EMBO J.* 2006;**25**:1207–18.
- 43 Okamoto K, Kashima K, Pereg Y, Ishida M, Yamazaki S, Nota A, et al. DNA damage-induced phosphorylation of MdmX at serine 367 activates p53 by targeting MdmX for Mdm2-dependent degradation. *Mol Cell Biol.* 2005;**25**:9608–20.
- 44 Pereg Y, Lam S, Teunisse A, Biton S, Meulmeester E, Mittelman L, et al. Differential roles of ATM- and Chk2-mediated phosphorylations of hdmx in response to DNA damage. *Mol Cell Biol.* 2006;**26**:6819–31.
- 45 He G, Zhang Y-W, Lee J-H, Zeng SX, Wang YV, Luo Z, et al. AMP-activated protein kinase induces p53 by phosphorylating MDMX and inhibiting its activity. *Mol Cell Biol.* 2014;**34**:148–57.

- 46 Pereg Y, Shkedy D, de Graaf P, Meulmeester E, Edelson-Averbukh M, Salek M, et al. Phosphorylation of Hdmx mediates its Hdm2- and ATM-dependent degradation in response to DNA damage. *Proc Natl Acad Sci USA*. 2005;**102**:5056–61.
- 47 Chen L, Gilkes DM, Pan Y, Lane WS, Chen J. ATM and Chk2-dependent phosphorylation of MDMX contribute to p53 activation after DNA damage. *EMBO J*. 2005;**24**:3411–22.
- 48 Feng J, Tamaskovic R, Yang Z, Brazil DP, Merlo A, Hess D, et al. Stabilization of Mdm2 via decreased ubiquitination is mediated by protein kinase B/Akt-dependent phosphorylation *. *J Biol Chem*. 2004;**279**:35510–7.
- 49 Ashcroft M, Ludwig RL, Woods DB, Copeland TD, Weber HO, MacRae EJ, et al. Phosphorylation of HDM2 by Akt. *Oncogene*. 2002;**21**:1955–62.
- 50 Milne D, Kampanis P, Nicol S, Dias S, Campbell DG, Fuller-Pace F, et al. A novel site of AKT-mediated phosphorylation in the human MDM2 onco-protein. *FEBS Lett*. 2004;**577**:270–6.
- 51 Zhou BP, Liao Y, Xia W, Zou Y, Spohn B, Hung M-C. HER-2/neu induces p53 ubiquitination via Akt-mediated MDM2 phosphorylation. *Nat Cell Biol*. 2001;**3**:973–82.
- 52 Mayo LD, Donner DB. A phosphatidylinositol 3-kinase/Akt pathway promotes translocation of Mdm2 from the cytoplasm to the nucleus. *Proc Natl Acad Sci USA*. 2001;**98**:11598–603.
- 53 Wood NT, Meek DW, MacKintosh C. 14-3-3 binding to Pim-phosphorylated Ser166 and Ser186 of human Mdm2 – potential interplay with the PKB/Akt pathway and p14ARF. *FEBS Lett*. 2009;**583**:615–20.
- 54 Yang HY, Wen YY, Lin YI, Pham L, Su CH, Yang H, et al. Roles for negative cell regulator 14-3-3 σ in control of MDM2 activities. *Oncogene*. 2007;**26**:7355–62.
- 55 Coblitz B, Wu M, Shikano S, Li M. C-terminal binding: an expanded repertoire and function of 14-3-3 proteins. *FEBS Lett*. 2006;**580**:1531–5.
- 56 Yaffe MB, Rittinger K, Volinia S, Caron PR, Aitken A, Leffers H, et al. The structural basis for 14-3-3: phosphopeptide binding specificity. *Cell*. 1997;**91**:961–71.
- 57 Milroy L-G, Brunsvelde L, Ottmann C. Stabilization and inhibition of protein-protein interactions: the 14-3-3 case study. *ACS Chem Biol*. 2012;**8**:27–35.
- 58 Madeira F, Tinti M, Murugesan G, Berrett E, Stafford M, Toth R, et al. 14-3-3-Pred: improved methods to predict 14-3-3-binding phosphopeptides. *Bioinformatics*. 2015;**31**:2276–83.
- 59 Zhang H, Wu Q, Berezin MY. Fluorescence anisotropy (polarization): from drug screening to precision medicine. *Expert Opin Drug Discov*. 2015;**10**:1145–61.
- 60 Yang X, Lee WH, Sobott F, Papagrigoriou E, Robinson CV, Grossmann JG, et al. Structural basis for protein–protein interactions in the 14-3-3 protein family. *Proc Natl Acad Sci USA*. 2006;**103**:17237–42.
- 61 Molzan M, Ottmann C. Synergistic binding of the phosphorylated S233- and S259-binding sites of C-RAF to one 14-3-3 ζ dimer. *J Mol Biol*. 2012;**423**:486–95.
- 62 Kalabova D, Smidova A, Petrvalska O, Alblova M, Kosek D, Man P, et al. Human procaspase-2 phosphorylation at both S139 and S164 is required for 14-3-3 binding. *Biochem Biophys Res Commun*. 2017;**493**:940–5.
- 63 Stevers LM, de Vink PJ, Ottmann C, Huskens J, Brunsvelde L. A Thermodynamic model for multivalency in 14-3-3 protein-protein interactions. *J Am Chem Soc*. 2018;**140**:14498–510.
- 64 Kuusk A, Neves JF, Bravo-Rodriguez K, Gunnarsson A, Ruiz-Blanco YB, Ehrmann M, et al. Adoption of a turn conformation drives the binding affinity of p53 C-terminal domain peptides to 14-3-3 σ . *ACS Chem Biol*. 2020;**15**:262–71.
- 65 Molzan M, Kasper S, Röglin L, Skwarczynska M, Sassa T, Inoue T, et al. Stabilization of physical RAF/14-3-3 interaction by cotylenin a as treatment strategy for RAS mutant cancers. *ACS Chem Biol*. 2013;**8**:1869–75.
- 66 Winn MD, Ballard CC, Cowtan KD, Dodson EJ, Emsley P, Evans PR, et al. Overview of the CCP4 suite and current developments. *Acta Crystallogr D*. 2011;**67**:235–42.
- 67 Emsley P, Lohkamp B, Scott WG, Cowtan K. Features and development of Coot. *Acta Crystallogr D*. 2010;**66**:486–501.
- 68 Kovalevskiy O, Nicholls RA, Long F, Carlon A, Murshudov GN. Overview of refinement procedures within REFMAC5: utilizing data from different sources. *Acta Crystallogr D*. 2018;**74**:215–27.
- 69 Schrodinger LLC. The PyMOL Molecular graphics system, version 1.8. 2015.

Supporting information

Additional supporting information may be found online in the Supporting Information section at the end of the article.

Fig. S1. Sequence alignment of 14-3-3 proteins.

Fig. S2. hDMX and hDM2 sequences.

Fig. S3. Sequence alignment for hDM2 and hDMX proteins.

Fig. S4. Fluorescence anisotropy assays for the hDM2 peptides.

Fig. S5. Fluorescence anisotropy assays for the hDMX₁₄₄₋₁₅₈^{pThr151} peptide with all isoforms of 14-3-3.

Fig. S6. Fluorescence anisotropy assays for unphosphorylated *hDMX* and *hDM2* peptides with 14-3-3 η .

Fig. S7. ITC data for the interaction of *hDMX* and *hDM2* peptides with 14-3-3 η .

Fig. S8. Dose–response SPR experiments for the binding of *hDMX* and *hDM2* peptides to immobilized 14-3-3 η .

Fig. S9. Data Fitting for dose–response SPR experiments for the binding of *hDMX* and *hDM2* peptides to immobilized 14-3-3 η .

Fig. S10. AUC data for 14-3-3 η and *hDMX*₃₃₅₋₃₇₄^{pSer342/pSer367}.

Fig. S11. Additional images for the *hDMX*₃₆₁₋₃₇₄^{pSer367}/1433 σ structure (PDB: 6YR5).

Fig. S12. Additional images for the *hDM2*₁₈₀₋₁₉₂^{pSer186}/1433 σ structure (PDB: 6YR6).

Fig. S13. *hDMX*₃₃₅₋₃₇₄^{pSer342/pSer367}/1433 σ structure (PDB ID: 6YR7).

Table S1. High-resolution mass spectrometry data for peptides.